

Magneto-electrodynamics at high frequencies in the antiferromagnetic and superconducting states of $\text{DyNi}_2\text{B}_2\text{C}$

Durga P. Choudhury and H. Srikanth

*Department of Physics, Northeastern University, Boston, Massachusetts 02115
and Air Force Research Laboratory, Hanscom Air Force Base, Bedford, Massachusetts 01730*

S. Sridhar

Department of Physics, Northeastern University, Boston, Massachusetts 02115

P. C. Canfield

*Ames Laboratory, Department of Physics and Astronomy, Iowa State University, Ames, Iowa 50011
(Received 15 October 1997)*

We report our observation of the behavior of the radio frequency (rf) and microwave response of $\text{DyNi}_2\text{B}_2\text{C}$ over a wide range of temperature (T) and magnetic field (H) in the antiferromagnetic (AFM) and superconducting (SC) states. At microwave frequencies of 10 GHz, the T dependence of the surface impedance $Z_s = R_s + iX_s$ was measured which yields the T dependence of the complex conductivity $\sigma_1 - i\sigma_2$ in the SC and AFM states. At radio frequencies (4 MHz), the H and T dependence of the penetration depth $\lambda(T, H)$ were measured. The establishment of antiferromagnetic order at $T_N = 10.3$ K results in a marked decrease in the scattering of charge carriers, leading to sharp decreases in R_s and X_s . However, R_s and X_s differ from each other in the AFM state. We show that the results are consistent with relaxation processes whence the scattering rate becomes comparable to the microwave frequency. The rf measurements yield a rich dependence of the scattering on the magnetic field near and below T_N . Anomalous decrease of scattering at moderate applied fields is observed at temperatures near and above T_N , and arises due to a crossover from a negative magnetoresistance state, possibly associated with a loss of spin disorder scattering at low fields, to a positive magnetoresistance state associated with the metallic nature. The normal state magnetoresistance is positive at all temperatures for $\mu_0 H > 2$ T and at all fields for $T > 15$ K. Several characteristic field scales associated with metamagnetic transitions [$H_{M1}(T)$, $H_{M2}(T)$], the onset of spin disorder $H_D(T)$ and the upper critical field $H_{c2}(T)$ are observed in the rf measurements. [S0163-1829(98)04342-2]

I. INTRODUCTION

The discovery of superconductivity in the quaternary borocarbides^{1,2} has led to a family of materials with intriguing properties. These are the only known intermetallic superconductors containing an appreciable amount of nickel that have transition temperatures in excess 10 K. Stoichiometric single phase compounds with the general composition of $\text{RNi}_2\text{B}_2\text{C}$, where R is a rare-earth element, yttrium or lutetium have been synthesized³ and extensively investigated. Most members of this family that exhibit superconductivity also have coexisting antiferromagnetic order, notable exceptions being $\text{YNi}_2\text{B}_2\text{C}$ and $\text{LuNi}_2\text{B}_2\text{C}$.⁴ This system therefore is very useful in studying the interplay between magnetism and superconductivity. The order in temperature in which these two transitions occur as well as the values of the relevant temperature scales associated (T_N for antiferromagnetic transition and T_c for superconducting transition) vary significantly. Although the monotonic decrease in superconducting transition temperature with increasing de Gennes factor of the rare earth is usually attributed to the pair breaking effects of the moments,⁵ the magnetism in these materials is much more complex and defies a simple explanation. For one thing, it turns out that the presence of nickel, hitherto thought to be grossly detrimental to superconductivity because of its pair breaking effects, is relatively benign in these

materials and does not contribute significantly to its magnetic properties.⁶ Most of the pair breaking comes from the rare-earth moments in these systems where they are present.

Recently, superconductivity ($T_c = 6.2$ K) was reported in $\text{DyNi}_2\text{B}_2\text{C}$, below an antiferromagnetic transition at $T_N = 10.3$ K.^{5,7} Thus this material is one of a select few materials where superconductivity appears in the presence of long-range magnetic order, some others being systems such as $\text{Ho}(\text{Ir}_x\text{Rh}_{1-x})_4\text{B}_4$,⁸ $\text{Tb}_2\text{Mo}_3\text{Si}_4$,⁹ and some of the heavy fermion superconductors.¹⁰

Metallic or superconducting antiferromagnets afford the possibility to study the influence of local moments on electronic properties. In the metallic state, interesting effects are expected on the transport properties such as the conductivity. In the superconducting state, magnetism can lead to novel effects on the superconducting order parameter. This is because of the presence of low energy and magnetic field scales in the system, such as spin-flop field scales arising from the magnetic state, and vortex-related fields due to superconductivity.

High-frequency measurements such as those of the surface impedance $Z_s = R_s + iX_s$ yield unique information often not available with other techniques, particularly those at dc or low frequencies such as dc resistivity or ac susceptibility. In the metallic state, information regarding the dynamics of electrons and electronic moments can be obtained. In the

superconducting state, the order parameter can be probed in terms of the penetration depth. Because of finite dissipation at high frequencies, one can simultaneously probe the quasi-particle effects too.

In this paper we report our results on measurements of radio frequency (~ 4 MHz) skin depth and microwave (~ 10 GHz) surface impedance on high-quality single crystals of this material. Several features are reported. A marked decrease in the scattering of charge carriers is observed upon establishment of antiferromagnetic order at $T_N = 10.3$ K. R_s and X_s differ from each other in the antiferromagnetic state, which we show arises from relaxation effects. Anomalous decrease of scattering at moderate applied fields is observed at temperatures near and above T_N , and is proposed to arise from changes in spin disorder scattering. Several characteristic field and temperature scales associated with metamagnetic transitions [$H_{M1}(T), H_{M2}(T)$] and a crossover field scale $H_D(T)$, in addition to T_c , T_N , and $H_{c2}(T)$ are observed in the rf measurements. The behavior of the complex conductivity in the SC and AFM state is obtained as a function of temperature.

II. EXPERIMENTAL DETAILS

A. rf setup

The rf measurements were carried out in a tunnel diode driven tank oscillator self-resonant typically at 4 MHz. The sample is placed in an inductive coil which is part of the L - C tank with the rf field H_{rf} , the dc field H_{dc} , and the \hat{c} axis oriented such that $H_{rf} \perp H_{dc} \perp \hat{c}$. The inset to Fig. 2 shows a picture of this geometry. Magnetic fields upto 70 kOe were applied using a superconducting magnet. This experimental technique has been extensively used to study high- and low- T_c superconductors both in the Meissner and mixed states.¹¹⁻¹³ If either the skin depth δ or the superconducting penetration depth λ changes as functions of T or H , these changes can be measured as changes Δf in resonant frequency using $\Delta(\delta \text{ or } \lambda) = -G\Delta f$, where G is a geometric factor. The oscillator is ultrastable (approximately 1 Hz in 4 MHz), and this leads to very high sensitivity, with typical resolutions of a few Å. Earlier experiments in cuprate superconductors have led to a wide variety of information regarding superconducting parameters such as the lower critical field H_{c1} and pinning forces κ_p (Ref. 11) and have also been recently used to study borocarbide superconductors where they have revealed features in the H - T phase diagram.^{12,13} The primary advantage of our technique is the ability to probe both the resistivity in the normal state and superfluid density in the superconducting state which is not possible with conventional techniques such as dc resistivity or ac susceptibility. An interesting example of the versatility and sensitivity of the setup was recently demonstrated when we could resolve an *area preserving* hexagonal to square transition of the flux line lattice in $\text{ErNi}_2\text{B}_2\text{C}$,¹⁴ another member of the borocarbide family, which was not visible in magnetic susceptibility measurements.

The sample was mounted on a sapphire rod with a groove machined on it. Sapphire is a good thermal conductor but a poor electrical conductor; thus while the sample is thermally well anchored to its environment, the contribution of the sample holder to the frequency shift is minimal. The coil was

mounted on the sapphire and was attached to a sheet of alumina with GE varnish. The alumina sheet carried an electric heater for fine tuning of the sample temperature. Data acquisition was done by a computer using a GPIB interface.

B. Microwave setup

The microwave measurements were carried out in a superconducting niobium cavity using the ‘‘cold cavity-hot finger’’ technique.¹⁵ The cavity is immersed in a bath of liquid helium, and the sample is mounted on a piece of sapphire inside the cavity. The sapphire has a heater mounted on it so that the temperature of the sample can be varied from below 4 K to above 200 K while the cavity is maintained at a fixed temperature of 4.2 K, as is necessary for it to remain superconducting. The perturbation of the cavity due to the change in the superconducting properties of the sample is reflected as a change of resonance frequency f and bandwidth δf of the cavity. This is related to the change in the complex surface impedance ($Z_s = R_s + iX_s$) as $R_s = \Gamma[1/Q_s(T) - 1/Q_0(T)]$ and $\Delta X_s = 2\pi\mu_0 f_0 \Delta\lambda = (-2\Gamma/f_0)[f_s(T) - f_0(T)]$, where Γ is a geometric factor relating to the cavity and the sample dimensions, Q_s and Q_0 are the loaded and unloaded quality factor of the cavity ($Q = f/\delta f$), and f_s and f_0 are the loaded and unloaded resonance frequencies, respectively. Our setup allows us to measure the absolute value of R_s but only the relative change in X_s . An absolute value is imposed on X_s by assuming that $X_s = R_s$ at high temperatures ($T \gg T_c, T_N$) where any effect of superconductivity or magnetism would be negligible. The superconducting cavity has very high Q , of the order of $10^7 - 10^8$, making it very sensitive to small changes in the surface resistance ($\sim 10 \mu\Omega$) and penetration depth (~ 1 Å). An additional advantage of the superconducting cavity is that it shields out stray magnetic fields from the sample. This technique has been very successfully used to yield a wealth of information on other members of the borocarbide family¹⁶ as well as many high-temperature superconductors.^{17,18}

C. Crystal growth

High-quality single crystals of the material were prepared using the high-temperature flux growth technique.¹⁹ This method consists of furnace heating a mass of stoichiometric polycrystalline material with an equal mass of Ni_2B flux in an inert atmosphere. Single crystals of the material grow into the flux in the shape of platelets. The crystals grown this way have relatively large size, making them particularly useful for measurement of bulk properties. The superiority of these crystals in terms of phase purity, proper stoichiometry and low density of defects has been verified by x-ray diffraction and other methods.⁵ Typical size of the crystal used in our experiments is $2 \times 0.8 \times 0.2$ mm³.

III. RESULTS AND DISCUSSION

A. Radio frequency measurements

These experiments, carried out for $2 \text{ K} < T < 100 \text{ K}$ and $0 < H < 70$ kOe essentially measure the real part of the complex electromagnetic penetration depth $\tilde{\lambda} = \sqrt{-i/\mu\omega\sigma}$ at radio frequencies. In the normal state, $\sigma = \sigma_n$ is the normal

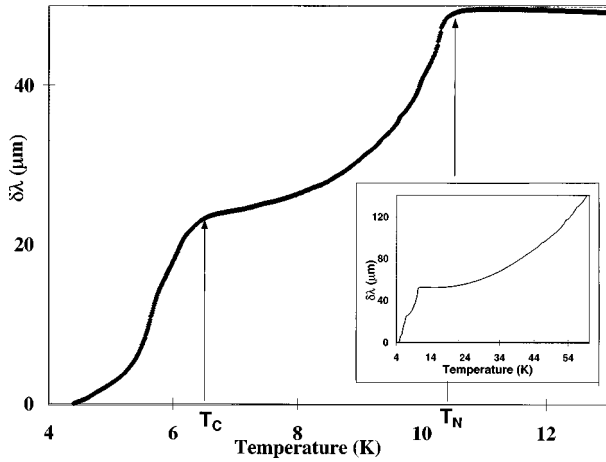


FIG. 1. Electromagnetic screening depth λ against temperature. The onset of superconductivity and the signature of the antiferromagnetic order are quite visible. Notice the similarity with Fig. 3(a) of Ref. 5 which is expected because of the proportionality between λ and $\sqrt{\rho}$. Inset: The same data shown over extended temperature range.

conductivity and is purely real. In this case, $\tilde{\lambda}^{-1} = \delta^{-1}(1 + i)$, where $\delta = \sqrt{2/\mu\omega\sigma_n}$ is the skin depth. In the superconducting state, σ has to be replaced with an effective complex conductivity $\sigma_s = \sigma_1 - i\sigma_2$ whose real and imaginary parts are proportional to the quasiparticle scattering and superfluid density, respectively. In the limit $\sigma_2 \gg \sigma_1$, which typically holds for $T < T_c$, $\tilde{\lambda} = 1/\sqrt{\mu\omega\sigma_2} = \lambda_L$, the London penetration depth. Notice that the normal state skin depth is a factor of $\sqrt{2}$ bigger than the penetration depth. All the data presented in this paper show penetration depths both in the normal and superconducting states and are denoted by λ .

The temperature dependence of λ shows a clear signature of the onset of the magnetic order at 10.3 K (see Fig. 1) which has also been observed by other techniques such as neutron scattering and specific heat measurements by other investigators.^{20–22} Onset of the superconducting transition brings about further decrease in magnetic field penetration. Note that measurement of dc resistivity also shows a very similar behavior⁵ which is to be expected because of the proportionality between the square root of resistivity and the skin depth as mentioned above. Although no details of temperature dependence of penetration depth in the superconducting state is visible in dc measurements because of the very nature of the technique, in our setup this information is clearly seen.

The same experiment, done in the presence of a finite dc field, reveals further interesting features. Figure 2 shows typical data taken for $H = 0, 2.5, 5,$ and 10 kOe, respectively. The inset shows the relative orientation of the sample's \hat{c} axis and the applied dc and rf fields. The direction of the induced rf current is also shown as a reference. Successive curves are shifted along the vertical axis by roughly the same amount to render greater clarity to the figure. Since in this experiment we only measure the *change* in screening length, a constant shift will not affect any of the further discussion. The total change in screening length is shown on the right-hand side of each curve. The superconducting transition is still visible but with a depressed T_c in the field-cooled $\lambda(T)$ curve at H

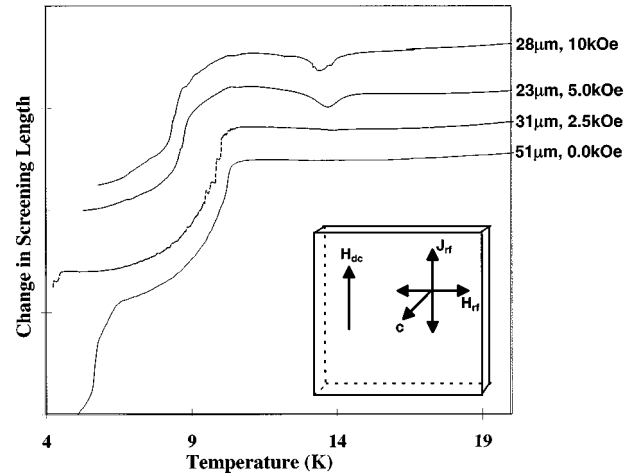


FIG. 2. Radio frequency penetration depth against temperature measured in finite magnetic field. Various data sets have been shifted from each other vertically for clarity of presentation. Inset: Schematic of sample orientation relative to H_{dc} and H_{rf} .

$= 2.5$ kOe. The application of a magnetic field decreases the sharpness of the change of λ at the antiferromagnetic transition and it appears that at a field greater than the zero temperature H_{c2} , the λ would attain a constant value independent of temperature at very low temperatures. This reflects the residual resistivity of the material. As temperature is increased, a dip appears in the screening length for field scales ~ 10 kOe. It signals the existence of some mechanism that leads to the reduction in scattering of charge carriers. We shall elaborate on that later in this paper.

To see these features from another perspective, we did a series of measurements of λ against H at various fixed temperatures and a few typical data sets are shown in Fig. 3. The plots for successively increasing temperatures have been displaced from each other along the vertical axis to avoid overlapping, as was done in Fig. 2. Several features of the field ramp data, although present in the temperature ramps, are now more obvious. We point them out in the following.

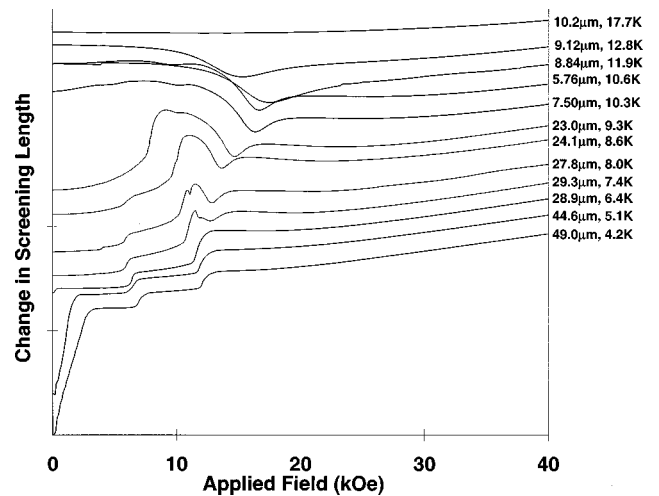
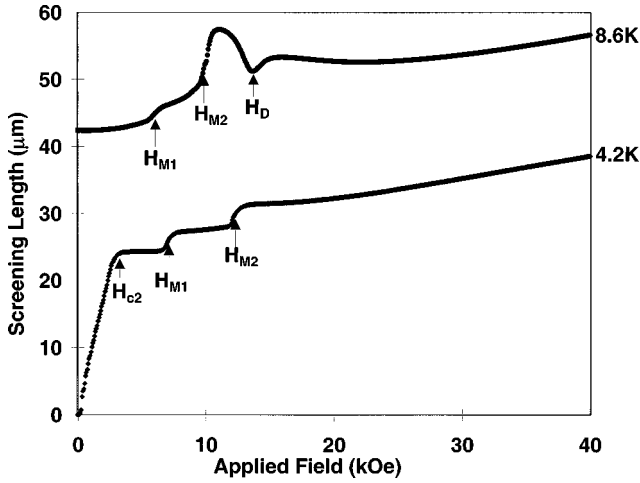


FIG. 3. Screening length against field at various temperatures. Each curve has been displaced along the vertical axis by a fixed amount for better visibility. The total change in screening length $[\lambda(H = 70 \text{ kOe}, T) - \lambda(H = 0, T)]$ is indicated on the right hand side for each curve.

FIG. 4. Characteristic field scales in $\text{DyNi}_2\text{B}_2\text{C}$.

The magnetic state shows two sharp jumps of the screening length both above and below T_c , originating from metamagnetic transitions in the sample. Such transitions have also been noticed in dc magnetization measurements of $\text{DyNi}_2\text{B}_2\text{C}$ (Refs. 21 and 23) as well as in other members of the borocarbide family such as $\text{HoNi}_2\text{B}_2\text{C}$.^{24–26} With the increase of temperature, the magnitude of the jump at field H_{M1} (as defined in Fig. 4) decreases and that of the one at H_{M2} increases.

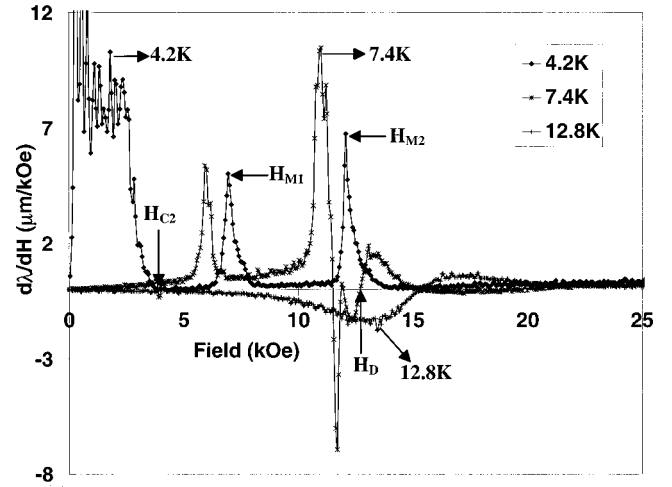
In the nonsuperconducting state, regardless of the magnetic order, the resistance goes through a local minimum as the field is swept from zero. The sharpness of this minimum goes down as temperature is increased, and at the highest temperature of 17.7 K at which data was taken, this minimum is barely visible. We remark here in passing that the data shown in Fig. 2 indicate that the field scale H_D (defined in Fig. 4) at which this dip is most pronounced decreases rapidly at $T \sim 13$ K.

The response of the material at very high field (>20 kOe) shows positive magnetoresistance at all temperatures, characteristic of its metallic behavior. Data are shown only upto 40 kOe in Fig. 3 for clarity of presentation. Beyond this, λ increases monotonically with field up to 70 kOe, the maximum field at which data was taken.

It is obvious from Fig. 3 that the screening length is characterized by field scales in addition to the well known scale of H_{c2} . In Fig. 4 we define the nomenclature for these field scales that we will subsequently be using for discussion throughout this paper. The two field scales corresponding to the metamagnetic transitions are called H_{M1} and H_{M2} , respectively, and the scale at which skin depth reaches a local minimum for $T > T_c$ ($H=0$) is called H_D .

To further analyze these features, we numerically calculated $d\lambda/dH$ for the data shown in Fig. 3. Three typical data sets of this kind, one each for the case of $T < T_c$, $T_c < T < T_N$ and $T > T_N$ are shown in Fig. 5. The characteristic field scales that we discussed above are now much more obvious.

The topic of the interplay between antiferromagnetism and superconductivity has been extensively investigated.^{27–33} Many of the ‘‘classic’’ antiferromagnetic superconductors such as the rhodium boride cluster compounds and RMo_8S_8 (R =rare earth) are well known to undergo field induced spin-flop transitions in the superconducting state which have

FIG. 5. $d\lambda/dH$ for $\text{DyNi}_2\text{B}_2\text{C}$ at different temperatures.

been investigated both experimentally³⁴ and theoretically.^{35,36} Such transitions in $\text{DyNi}_2\text{B}_2\text{C}$, however, occur at H_{M1} and H_{M2} ($>H_{c2}$) after superconductivity has been quenched, either by raising temperature or the applied field.

Above T_N , the magnetoresistance of this material goes through a local minimum with increasing field (Fig. 3), the sharpness of which decreases as temperature increases. Although at first inspection this local minimum in magnetoresistance may appear quite novel, we believe that it is associated with a crossover from the negative magnetoresistance associated with the loss of spin disorder scattering from the Dy sublattice as it is aligned along the applied field to the positive magnetoresistance associated with conduction band electrons. These two effects are clearly seen in data taken in the paramagnetic state of $\text{HoNi}_2\text{B}_2\text{C}$ and $\text{LuNi}_2\text{B}_2\text{C}$.^{37,38} Although these two effects do indeed give rise to a local minimum in magnetoresistance in the paramagnetic state they do not give rise to as sharp a local minimum as is seen in the data in Fig. 3. This enhanced sharpness may be associated with interaction between the local moments since $T \approx T_N$ for these data. Another possible explanation for the local minimum is that it represents an as-of-yet undetected phase transition line that exists at intermediate fields for a temperature near T_N . Although we currently consider this to be the less likely explanation, the possibility of another phase transition is the subject of ongoing research.

From the data of Fig. 5, we constructed a ‘‘phase diagram’’ for $\text{DyNi}_2\text{B}_2\text{C}$ demarcating the temperature dependence of the various field scales as shown in Fig. 6. H_{c2} was defined to be the field at which $d\lambda/dH$ becomes vanishingly small. The values thus obtained are somewhat higher than those obtained from dc measurements.⁵ The same criterion was used for determining H_D , the field at which λ goes through a minimum. It is worth mentioning here that H_D most likely a crossover field scale and does not represent a phase transition as was discussed previously. H_{M1} and H_{M2} , however, represent field scales corresponding to metamagnetic transitions³⁹ and are chosen so that $d\lambda/dH$ is maximum. The region within the full width at half maximum of each peak is shaded in the diagram demarcating the approximate span of the transition region.

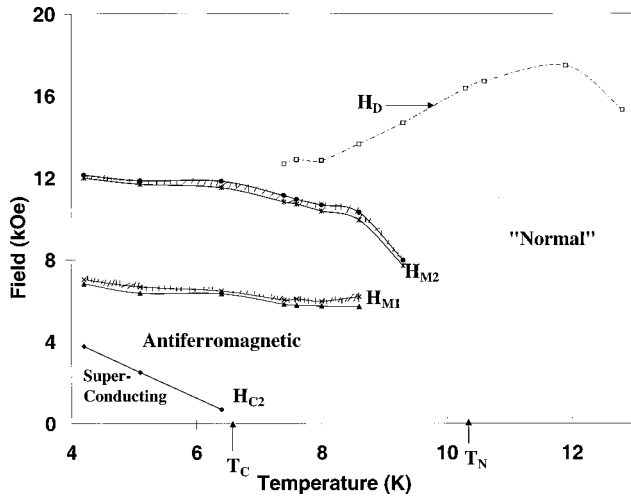


FIG. 6. Temperature dependence of characteristic field scales in $\text{DyNi}_2\text{B}_2\text{C}$. The shaded regions demarcate the regimes of the two metamagnetic transitions. The lines joining the data points are meant to be a guide to the eye.

B. Microwave measurements

Figure 7 shows the surface impedance at 10 GHz as a function of temperature. For a normal metal, the real and imaginary parts of the surface impedance are equal, as is obvious from elementary electrodynamic considerations,⁴⁰ and indeed such behavior is observed in the normal state for all the materials we have studied in our setup so far. However, $\text{DyNi}_2\text{B}_2\text{C}$ is unique in the sense that R_s and X_s (where $Z_s = R_s + iX_s$) differ from each other even in the AFM state below T_N .

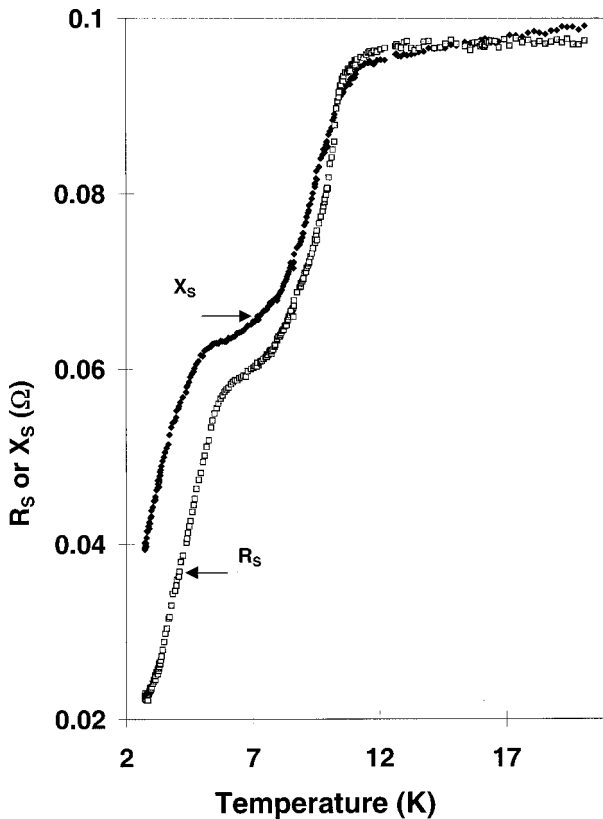


FIG. 7. The real and imaginary parts of the microwave surface impedance of $\text{DyNi}_2\text{B}_2\text{C}$ as a function of temperature.

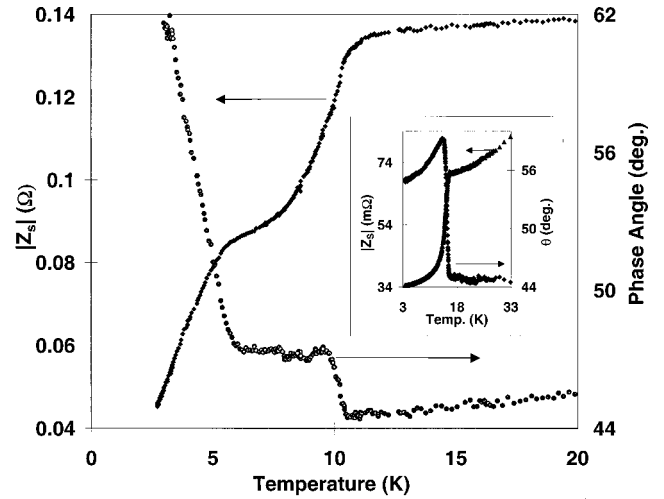


FIG. 8. The magnitude and phase angle of microwave surface impedance of $\text{DyNi}_2\text{B}_2\text{C}$ as a function of temperature. Inset: The same quantities measured on a single crystal of $\text{YNi}_2\text{B}_2\text{C}$, from Ref. 16.

To see this from another perspective, we have plotted the absolute value of the surface impedance $Z_s(T) = \sqrt{R_s^2 + X_s^2}$ and the phase angle $\theta(T) = \tan^{-1}(X_s/R_s)$ in Fig. 8. Although there is an overall similarity of shape of Z_s vs T between the microwave measurements and the ones measured using the radio frequency technique and the usual four-probe dc resistivity, the microwave measurements yield additional information. For a “conventional” superconductor, the phase angle is expected to change sharply from 45° in the normal state tending towards 90° as $T \rightarrow 0$ below the superconducting transition temperature, and such transitions have indeed been observed by us for most types of superconductors. Typical data for a single crystal of $\text{YNi}_2\text{B}_2\text{C}$ (Ref. 16) is shown in the inset of Fig. 8 for reference. In the case of $\text{DyNi}_2\text{B}_2\text{C}$ the phase angle starts to increase relatively sharply at the onset of the antiferromagnetic transition and continues to increase for about 0.5 K below T_N below which it becomes flat again until the superconducting transition sets in. The deviation of θ from 45° even before the superconducting transition is a possible manifestation of relaxation effects and is discussed in the following. Below the superconducting transition at T_c , θ rises as T is decreased as is expected for a superconductor.

1. Relaxation phenomena in the AFM state

While extensive amount of research has been carried out on magnetic properties of rare-earth metals and alloys,^{41,42} experimental data on their high-frequency electromagnetic response remain scant. The anomalous behavior of Z_s in the antiferromagnetic state could originate from a number of different physical phenomena, including an anomalous skin effect similar to that in conventional metal, a Drude-type conductivity relaxation [i.e., $\sigma(\omega) = \sigma_0/(1 + i\omega\tau)$, where σ_0 is the dc conductivity], and dissipation because of magnetic relaxation effects, giving rise to a complex permeability ($\mu/\mu_0 = \mu_1 + i\mu_2$).

While it is impossible to definitively rule out any one of these mechanisms in favor of the other based on our experimental data alone, conclusions can be drawn based on physi-

cally plausible assumptions. The first two possibilities are somewhat related to each other. For the material to be in the anomalous skin effect regime, the mean free path has to be comparable to the skin depth. From the measured dc resistivity⁵ the skin depth at 10 GHz and 11 K is estimated to be $\sim 1.1 \mu\text{m}$. Since the mean free path of comparably good metals is at least an order of magnitude lower, it has to increase by that much at the onset of the antiferromagnetic transition. For a Drude-type conductivity relaxation to manifest itself, the scattering time $\tau \sim 1/\omega = 10^{-10}$ s. Again, this is at least an order of magnitude lower in metals of comparable conductivity.

Although a temperature-dependent complex permeability does occur in antiferromagnetic and ferrimagnetic insulators, it is presumable that in a good metal such as DyNi₂B₂C conduction electron scattering will dominate over spin relaxation effects. This is reflected in the fact that zero field dc conductivity is profoundly affected by the onset of magnetic order.⁵ Even in case of a complex permeability, changes in its real part can generally be ignored in our system because of lack of macroscopic moment as well as the fact that the microwave magnetic field in our setup was parallel to the *c* axis of the crystal. Since the moments in this system are known to be coupled antiferromagnetically along the *c* axis, the temperature dependence of the in-phase component of the susceptibility would be minimal. Thus the dynamic permeability can be written as $\mu/\mu_0 = 1 + i\mu_2$.

Losses of magnetic origin can emanate from either a damped resonance or moment relaxation and both are observed in high-frequency response of ferrites^{43,44} and other magnetic systems.⁴⁵ However, let us point out here that the high values of μ_2 observed in ferrites is a measure of the *total* loss in the material which are usually due to eddy current, magnetic hysteresis, domain wall motion, and spin relaxation. In our case, transport current losses have been explicitly taken into account by the conductivity term and hysteretic and domain wall losses in a single crystal of an antiferromagnetic material in the absence of applied dc field, if at all present, is expected to be vanishingly small. Thus most of the losses in our case is attributable to the conductivity, with a possible small contribution from spin dynamics to account for the difference between R_s and X_s . Note that a frequency-dependent complex conductivity of the Drude type ($\sigma = \sigma_0/(1 + i\omega\tau)$) is algebraically equivalent to a dynamic permeability $\mu = \mu_1 + i\mu_2 = \mu_0(1 + i\omega\tau)$, so that $\mu_1 = \mu_0$ and $\mu_2 = \mu_0\omega\tau$. This kind of ambiguity between the electric and magnetic contribution to a measured physical quantity is characteristic of most dynamic measurements. Note that our rf measurements too effectively measure μ/σ . While both of our measurement techniques are significantly more sensitive compared to static experiments as has been discussed earlier in this paper, isolating the electric and magnetic contribution to the measured quantity has to be accomplished through comparison with the results of the static experiments and/or through physically consistent analysis. The scattering of conduction electrons by spin waves in the AFM state can give rise to the conductivity relaxation observed here. Conductivity relaxation is also observed in other cases such as spin density wave systems⁴⁶ and heavy fermion metals.⁴⁷

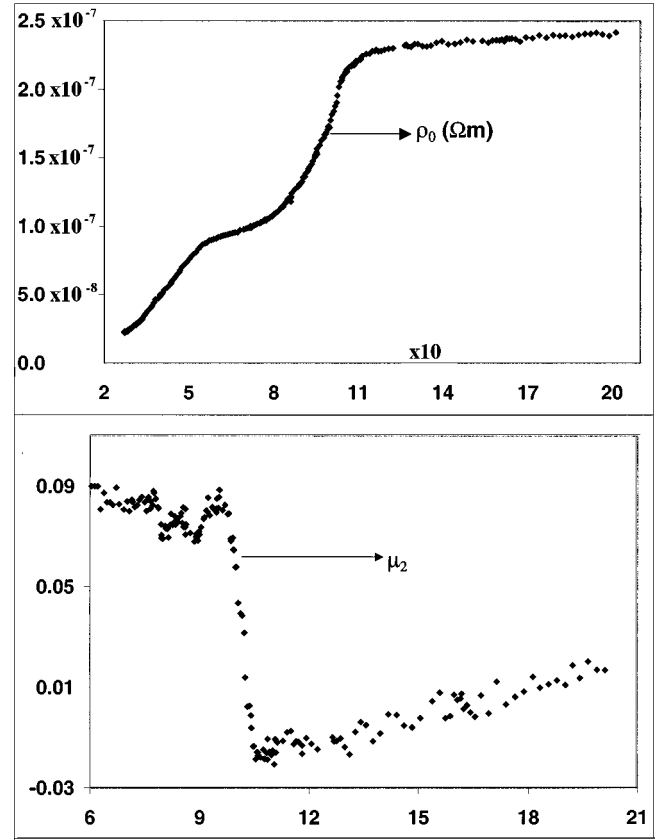


FIG. 9. Temperature dependence of some of the material parameters of DyNi₂B₂C. Top: Extracted dc resistivity ρ_0 . Bottom: The imaginary part of the permeability μ_2 .

Assuming a dynamic permeability of the form $\mu(T) = \mu_0(1 + i\mu_2)$, we have $Z_s = \sqrt{i\mu\omega/\sigma} = (\mu_0\omega/\sigma)^{1/2}(i - \mu_2)^{1/2}$, and the temperature dependence of $\mu_2(T) = (X_s^2 - R_s^2)/2X_sR_s$ in the region $T_c < T < 21$ K. The resulting $\mu_2(T)$ is shown in the bottom panel of Fig. 9. Also shown in the same figure on the top is $\rho_0 = 1/\sigma_0 = 2R_sX_s/\mu_0\omega$.

For $T > T_N$, $\mu_2 \rightarrow 0$, consistent with $R_s = X_s$ in the normal state. In the AFM state for $T < T_N$, μ_2 increases with decreasing T , saturating at a value of around 0.09.

2. Superconducting state

Since μ_2 is more or less temperature independent for $T_N > T > T_c$ other than the sharp change in the immediate vicinity of T_N , we can plausibly assume that this quantity remains independent of temperature even below T_c in the superconducting state. Since $\mu_2 \sim 0.09$ around T_c , the “effective” conductivity below T_c is assumed to be given by $\sigma_{s,\text{eff}} = \sigma_{1,\text{eff}} - i\sigma_{2,\text{eff}} = (\sigma_1 - i\sigma_2)/(1 + 0.09i)$. The real part of the effective conductivity takes into account the total dissipation in the system from all possible mechanisms, one of which can be the effect of spin relaxation. Similarly, the imaginary part of the effective conductivity includes all mechanisms of dissipation-free current flow in the system. Thus we are renormalizing the frequency-dependent conductivity in the superconducting state from the AFM state. The resulting temperature dependence of $\sigma_{1,\text{eff}}$ and $\sigma_{2,\text{eff}}$ in the superconducting state are shown in Fig. 10. Notice that $\sigma_{2,\text{eff}} = 0$ for $T > T_c$ which indicates that this quantity is the

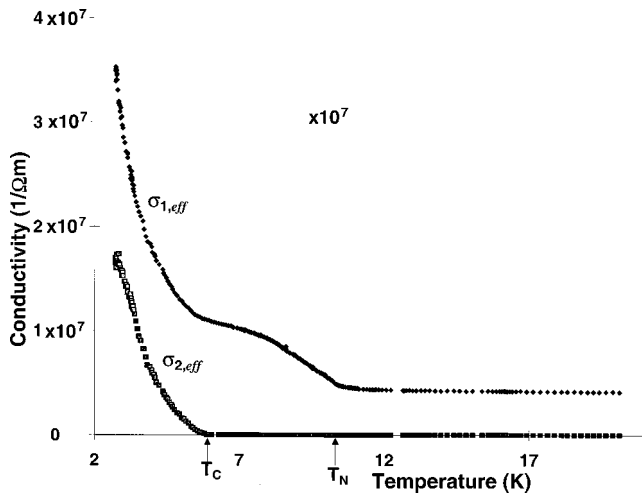


FIG. 10. The “effective” values of σ_1 and σ_2 .

correct measure of the superfluid density in the system. In the superconducting state, the temperature dependence of $\sigma_{2,eff}$ is anomalously broad and possibly arises out of strong pair breaking effects.⁴⁸ This is evident from the fact that $\sigma_{2,eff}$ continues to rise even for $T < T_c/2$, atypical of a “conventional” superconductor. A broad normal to superconducting transition is also observed in rf penetration depth (see Fig. 1) and dc resistivity measurements.^{5,49} Thus although antiferromagnetism does not inhibit the formation of the superconducting state, it appears to have a strong effect on the electrodynamic properties.

IV. CONCLUSION

In summary, a comprehensive set of measurements of the electrodynamic properties of DyNi₂B₂C in the radio fre-

quency and microwave regimes have been carried out, revealing some very interesting effects of magnetic and superconducting order on transport properties. The presence of magnetic Dy⁺³ ions strongly affects the transport properties. In the AFM state, establishment of long-range magnetic order leads to a strong reduction in scattering. Establishment of antiferromagnetic order gives rise to anomalous increase of electron scattering time which makes the real and imaginary parts of complex microwave surface impedance differ from each other. We have interpreted this behavior in terms of relaxation effects related to either charge transport or spin dynamics in the AFM state.

Antiferromagnetism also has a distinctive signature on the radio frequency skin depth measurements. Two field induced metamagnetic transitions were observed in the antiferromagnetic state at temperatures below T_N . A theoretical framework taking into account the scattering of the conduction electrons from the two-dimensional sheets of ferromagnetically coupled rare-earth moments is likely to be required for a clear understanding of all the observed effects. While several interesting results have emerged from the present measurements, the results also suggest new avenues to explore in further work and also call for a better theoretical understanding of these materials.

ACKNOWLEDGMENTS

Stimulating discussions with Balam A. Willemsen, S. Oxx, Benjamin Revcolevschi, T. Jacobs, A. Widom, R. Marckiewicz, and J. Sokoloff are thankfully acknowledged. This research was supported by the National Science Foundation through Grant No. 9623720.

- ¹R. Nagarajan, Chandan Mazumdar, Zakir Hossain, S. K. Dhar, K. V. Gopalakrishnan, L. C. Gupta, C. Godart, B. D. Padalia, and R. Vijayaraghavan, *Phys. Rev. Lett.* **72**, 274 (1994).
- ²R. J. Cava, H. Takagi, B. Battlog, H. W. Zandbergen, J. J. Krajewski, W. F. Peck, Jr., R. B. van Dover, R. F. Felder, T. Siegrist, K. Mizuhaski, J. O. Lee, H. Eisaki, S. A. Carter, and S. Uchida, *Nature (London)* **367**, 146 (1994).
- ³R. J. Cava, H. Takagi, B. Battlog, H. W. Zandbergen, J. J. Krajewski, W. F. Peck Jr., T. Siegrist, R. B. van Dover, R. F. Felder, K. Mizuhaski, J. O. Lee, H. Eisaki, S. A. Carter, and S. Uchida, *Nature (London)* **367**, 252 (1994).
- ⁴H. Eisaki, H. Takagi, R. J. Cava, K. Mizuhashi, J. O. Lee, S. Uchida, B. Battlog, J. J. Krajewski, and W. F. Peck Jr., *Phys. Rev. B* **50**, 647 (1994).
- ⁵B. K. Cho, P. C. Canfield, and D. C. Johnston, *Phys. Rev. B* **52**, R3844 (1995).
- ⁶M. E. Massalami, S. L. Budko, B. Giordanengo, and E. M. Baggio-Saitovitch, *Physica C* **244**, 41 (1995).
- ⁷C. V. Tomy, G. Balakrishnan, and D. M. Paul, *Physica C* **248**, 349 (1995).
- ⁸H. C. Ku, F. Acker, and B. T. Matthias, *Phys. Lett.* **76A**, 399 (1980).
- ⁹F. G. Aliev, Yu. K. Gorelenko, V. V. Pryadun, S. Vieira, R. Villar, and J. Paredes, *Physica B* **194-196**, 171 (1994).
- ¹⁰G. Aeppli, E. Bucher, C. Broholm, J. K. Kjems, J. Baumann, and J. Hufnag, *Phys. Rev. Lett.* **60**, 615 (1988).
- ¹¹D.-H. Wu and S. Sridhar, *Phys. Rev. Lett.* **65**, 2074 (1990).
- ¹²S. Oxx, D. P. Choudhury, B. A. Willemsen, H. Srikanth, S. Sridhar, P. C. Canfield, and B. K. Cho, *Physica C* **264**, 103 (1996).
- ¹³S. Sridhar, S. Oxx, Balam Willemsen, H. Srikanth, and D. P. Choudhury, *Phys. Rev. Lett.* **77**, 2145 (1996).
- ¹⁴M. R. Eskildsen, P. L. Gammel, B. P. Barber, U. Yaron, A. P. Ramirez, D. A. Huse, D. J. Bishop, C. Bolle, C. M. Lieber, S. Oxx, S. Sridhar, N. H. Andersen, K. Mortensen, and P. C. Canfield, *Phys. Rev. Lett.* **78**, 1968 (1997).
- ¹⁵S. Sridhar and W. L. Kennedy, *Rev. Sci. Instrum.* **59**, 531 (1988).
- ¹⁶T. Jacobs, Balam A. Willemsen, S. Sridhar, P. C. Canfield, and B. K. Cho, *Phys. Rev. B* **52**, R7022 (1995).
- ¹⁷T. Jacobs, S. Sridhar, Qiang Li, G. D. Gu, and N. Koshizuka, *Phys. Rev. Lett.* **75**, 4516 (1995).
- ¹⁸H. Srikanth, B. A. Willemsen, T. Jacob, S. Sridhar, A. Erb, E. Walker, and R. Flükiger, *Phys. Rev. B* **55**, R14 733 (1997).
- ¹⁹M. Xu, P. C. Canfield, J. E. Ostenson, D. K. Finnemore, B. K.

- Cho, Z. R. Wang, D. C. Johnston, and D. E. Farrell, *Physica C* **227**, 321 (1994).
- ²⁰P. Dervenagas, J. Zarestky, C. Stassis, A. I. Golman, P. C. Canfield, and B. K. Cho, *Physica B* **212**, 1 (1995).
- ²¹M. S. Lin, J. H. Shieh, Y. B. You, Y. Y. Hsu, J. W. Chen, S. H. Lin, Y. D. Yao, Y. Y. Chen, J. C. Ho, and H. C. Ku, *Physica C* **249**, 403 (1995).
- ²²J. W. Lynn, Q. Huang, S. K. Sinha, Z. Hossain, L. C. Gupta, and R. Nagarajan, *Physica B* **223&224**, 66 (1996).
- ²³P. C. Canfield and S. L. Bud'ko, *J. Alloys Compnd.* (to be published).
- ²⁴S. Oxx, D. P. Choudhury, H. Srikanth, S. Sridhar, and P. C. Canfield (unpublished).
- ²⁵P. C. Canfield, B. K. Cho, D. C. Johnston, D. K. Finnemore, and M. F. Hundley, *Physica C* **230**, 397 (1994).
- ²⁶P. C. Canfield, S. L. Bud'ko, B. K. Cho, A. Lacerda, D. Farrell, E. Johnston-Halperin, V. A. Kalatsky, and V. L. Pokrovsky, *Phys. Rev. B* **55**, 970 (1997).
- ²⁷A. I. Buzdin and L. H. Bulaevskii, *Sov. Phys. Usp.* **29**, 412 (1986).
- ²⁸M. B. Maple, *Physica B* **215**, 110 (1995).
- ²⁹R. Konno, *Physica B* **206&207**, 638 (1995).
- ³⁰M. B. Maple and Ø. Fischer, *Superconductivity in Ternary Compounds II: Superconductivity and Magnetism*, Vol. 34 of *Topics in Current Physics* (Springer-Verlag, New York, 1982).
- ³¹M. L. Kulić, A. I. Lichtenstein, E. Goreatchkovski, and M. Mehring, *Physica C* **244**, 185 (1995).
- ³²T. Ishiguro, Y. V. Sushko, H. Ito, and G. Saito, *J. Supercond.* **7**, 657 (1994).
- ³³M. A. Jensen and H. Suhl, in *Magnetism*, edited by G. T. Rado and H. Suhl (Academic, New York, 1996), Vol. IIB, Chap. 2, pp. 183–214.
- ³⁴H. Iwasaki, M. Ikebe, and Y. Muto, *Phys. Rev. B* **33**, 4669 (1986).
- ³⁵A. I. Buzdin, S. S. Krotov, and D. A. Kuptsov, *Solid State Commun.* **75**, 229 (1990).
- ³⁶O. Wong, H. Umezawa, and J. P. Whitehead, *Physica C* **158**, 32 (1989).
- ³⁷I. R. Fisher *et al.*, *J. Low Temp. Phys.* **105**, 1623 (1996).
- ³⁸I. R. Fisher, J. R. Cooper, and P. C. Canfield, *Phys. Rev. B* (to be published).
- ³⁹Z. Hossain, L. C. Gupta, R. Nagarajan, S. K. Dhar, C. Godart, and R. Vijayaraghavan, *Physica B* **223&224**, 99 (1996).
- ⁴⁰J. D. Jackson, *Classical Electrodynamics*, 2nd ed. (Wiley, New York, 1975).
- ⁴¹A. Arrott, in *Magnetism* (Ref. 33), Vol. IIB, Chap. 4, pp. 295–416.
- ⁴²J. Pierre, in *Magnetism of Metals and Alloys*, edited by M. Cyrot (North-Holland, New York, 1982), pp. 245–293.
- ⁴³M. Sodha and N. Srivastava, *Microwave Propagation in Ferrimagnetics* (Plenum, New York, 1981).
- ⁴⁴D. J. Craik, *Structure and Properties of Magnetic Materials* (Pion, London, 1971).
- ⁴⁵S. E. Lofland, S. M. Bhagat, S. D. Tyagi, Y. M. Mukovskii, S. G. Karabashev, and A. M. Balbashov, *J. Appl. Phys.* **80**, 3592 (1996).
- ⁴⁶H. H. S. Javadi, S. Sridhar, G. Grüner, Long Chiang, and F. Wudl, *Phys. Rev. Lett.* **55**, 1216 (1985).
- ⁴⁷S. Donovan, A. Schwartz, and G. Grüner, *Phys. Rev. Lett.* **79**, 1401 (1997).
- ⁴⁸B. K. Cho, P. C. Canfield, and D. C. Johnston, *Phys. Rev. Lett.* **77**, 163 (1996).
- ⁴⁹C. V. Tomy, M. R. Lees, L. Afalfiz, G. Balakrishnan, and D. McK. Paul, *Phys. Rev. B* **52**, 9186 (1995).